Studies of sidescatter and backscatter from pre-ionized plasmas

M. J. Herbst,[a] C. E. Clayton, W. A. Peebles, and F. F. Chen

University of California, Los Angeles, California 90024
(Received 22 October 1979; accepted 18 April 1980)

Stimulated Brillouin scattering at 180° and sidescatter at 90° are observed when CO_2 laser light is incident on an arc-pre-ionized, underdense plasma target. Scattering occurs in short spikes, sometimes early in the pulse, sometimes delayed by as much as 700 nsec. This time behavior depends critically on the state of pre-ionization and is explained by the evolution of a laser-driven ionization wave. Using ruby laser interferometry, it is possible to infer the sources of backscatter and sidescatter within this disturbance. In addition, by using a smooth input pulse, it is found that the spikiness of Brillouin scatter is not due solely to mode beating in the input beam.

I. INTRODUCTION

Of great importance to the success of the laser-pellet[1] or laser-heated, magnetically confined plasma[2] approaches to controlled fusion is the efficiency with which incident laser energy is coupled into the plasma. At the high laser intensities required for these schemes, parametric instabilities[3] such as the reflective stimulated Brillouin scattering process[4] may play a large role in determining this efficiency.

Stimulated Brillouin scattering has been observed in several experiments[5-12] using CO_2 laser radiation incident on gas or plasma targets with densities below the critical density $n_c \equiv m\omega_0^2/4\pi e^2$, so that complicating processes occurring at the critical layer are removed. The temporal evolution of the scattered light usually shows a prompt feature near the peak of the incident pulse, but several more unexpected characteristics have also been seen. The time of scattering and number of pulses seem to vary with the f number or focal length of the focusing optics.[6,7] Delayed scatter, occurring in the tail of the incident pulse, hundreds of nsec after the peak, has occasionally been seen.[5,6] In pre-ionized plasma targets, the scattered power depends sensitively on the time between the pre-ionization pulse and the laser pulse.[5] Both prompt and late scatter show a spikiness which has been attributed to self-mode-locking in the incident beam,[5,6] phase jumps in the beam,[5,7] or plasma turbulence.[7]

In the present work, we have attempted to explain all of these features except the f-number dependence. While previous investigations have concentrated on backscatter, the simultaneous observations of sidescatter and Brillouin backscatter[13] in this experiment have proved useful in identifying the scattering sources. Laser interferometry is used to measure the density and shape of the laser-altered plasma near the focus. It is found that the characteristics of this plasma depend sensitively on the pre-ionization level, as corroborated by optical spectroscopy. The long delays involved in late scatter are found to be explained by the evolution of the laser-altered plasma. Finally, by using cw injection to smooth the input pulse, the spikiness of stimulated Brillouin scattering is found to be not entirely due to the self-mode-locked spikes in the incident beam.

II. EXPERIMENTAL SETUP

The laser system used in this investigation is shown schematically in Fig. 1. The pulsed laser chain consists of an oscillator, a preamplifier, and a triple-passed power amplifier. Multimode gain-switched output energy of this chain is 30 J; since half of the energy is contained in a 50 nsec spike, peak power is 300 MW. In order to generate smoothed pulses for study of backscatter spikiness, a grating-tuned cw CO_2 laser producing 1.5 W on the $P(20)$ line of the 10.6 μm band of the CO_2 molecule is used. The output of this cw injection laser is focused through a hole in the rear reflector of the oscillator cavity to encourage narrow-band operation of that module. In this mode of operation, the length of the gain-switched spike increases and the peak power output of the chain drops to 200 MW. Typical output pulses with and without cw injection may be seen later in the upper traces of Figs. 2 and 3, respectively. The smoothness of the pulses shown with cw injection is not due to detector bandwidth limitation, since the same detector has been used to observe actively mode-locked CO_2 pulses of 1.5 nsec full width at the half-power points (FWHM).

The laser output is approximately 10 cm in diameter, with a central hole approximately 3.5 cm in diameter due to the Cassegrain configuration of the triple-pass beam expander on the power amplifier. This beam is focused by a 70 cm focal length antireflection coated germanium lens into the vacuum vessel of a pulsed hydrogen arc plasma source, as shown in Fig. 4. The discharge, which has been described previously,[5] is orthogonal to the plane of the figure, so that the CO_2 light is focused side-on into the plasma. The focus is at the edge of the arc plasma column, approximately 2 cm upstream (toward the laser) from the center of the arc, where the sidescatter collection lens is focused. This feature of the optical alignment will be important for explaining delayed scatter.

In the absence of plasma, the focal spot diameter is about 540 μm at the half-power points, giving a vacuum

[a] Present address: Naval Research Laboratory, Washington, D. C. 20375.

 0031-9171/80/071319-07$00.90

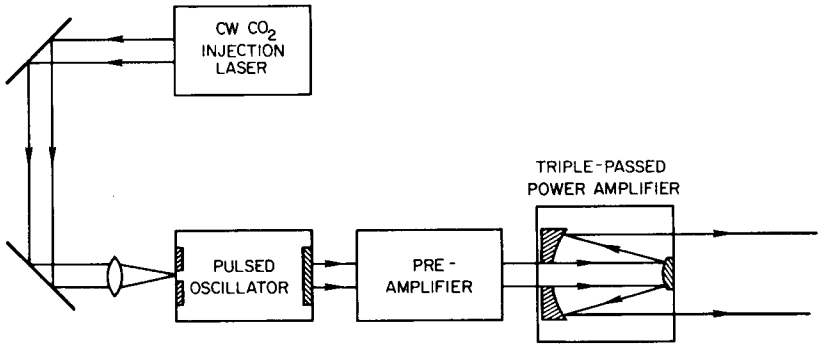

FIG. 1. CO_2 laser system.

intensity of 1.3×10^{11} W/cm^2. The portion of the beam transmitted by the plasma is dumped on a canted sheet of Plexiglas. Plasma diagnosis by visible spectroscopy is performed by viewing along the CO_2 input axis through this beam dump. The light collected in this manner is analyzed using a 2 m spectrograph and a gated optical multichannel analyzer.

Sidescatter is usually observed along the axis shown in Fig. 4, although it is also possible to view it along the axis of the arc through the hollow electrodes. Collected by a 12.5 cm focal length ZnSe lens focused at the center of the arc, this light is directed to the infrared detection system consisting of two liquid-helium cooled photoconductive detectors. Spectral analysis of scattered light is achieved by shot-to-shot scanning of a Fabry-Perot interferometer, with the total scattered light level being monitored by the second channel to remove shot-to-shot variation in that quantity from the data. The finesse of the interferometer is about 7; this low value prevents acquisition of information concerning spectral widths of scattered light, but allows measurement of any shifts from the incident laser frequency. The experimental arrangement for study of backscatter is identical to that for sidescatter, except that a beam splitter is inserted in the incident beam line between the laser power amplifier and the input focusing lens to sample backscattered light. This collected light may be directed to the infrared detectors for spectral analysis.

Plasma diagnosis by holographic interferometry is also accomplished along the sidescatter collection axis. Single mode pulses of 30 nsec FWHM from a ruby laser allow coarse time resolution of the laser-altered plasma evolution on a shot-to-shot basis. Between the first and second ruby pulse required to produce each interferogram, fill gas is changed in a hollow wedge in the reference beam path to introduce background fringes with 1.5 mm spacing. All imaging of the plasma onto the film plane is with unity magnification, so that the background fringe spacing in the plasma is also 1.5 mm. More finely spaced fringes are not justified at the present ruby pulse width, because the motion of the laser-altered plasma during the ruby laser pulse still limits spatial resolution.

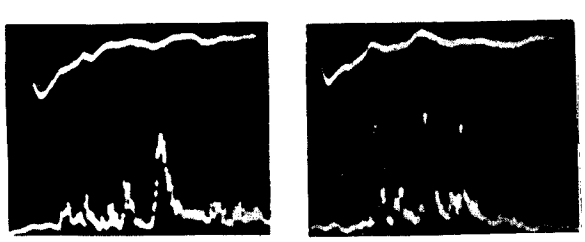

FIG. 2. Backscatter using smoothed CO_2 input pulse on 50 nsec/div sweeps. Upper traces are input pulses (75 MW/div) and lower traces are backscatter (approximately 400 W/div).

III. RESULTS

A. Backscatter observations

Time histories of backscattered light are of two types: prompt backscattering may occur within 50 nsec of the laser peak, or tail backscattering may take place at any time from 100 to 700 nsec after the laser peak. This agrees well with previous observations of backscatter from this device.[5] It is found that the time of occurrence of backscatter is correlated with the initial level of ionization due to the arc, and that this level is controllable by adjusting the time between the firing of the arc and of the CO_2 laser. Higher levels of pre-ionization lead to prompt scattering; lower levels to delayed scattering. Shown in Fig. 3 are examples of prompt backscatter observed with more pre-ionization and late backscatter observed with less pre-ionization.

Both prompt and late backscatter are found to be redshifted from the incident laser frequency by 14.8 ± 1.2 GHz and 18.5 ± 1.5 GHz, respectively. The prompt backscatter shift, coupled with an estimated[14] $T_e/T_i \simeq 4$, implies that $T_e=37\pm6$ eV and that $T_i=9.2\pm1.5$ eV at the time of prompt backscatter. By the time of late backscatter, electron-ion equilibration should have occurred. One then infers that $T_e\simeq T_i=25\pm4$ eV at the time of the measured late backscatter shift, 400 to

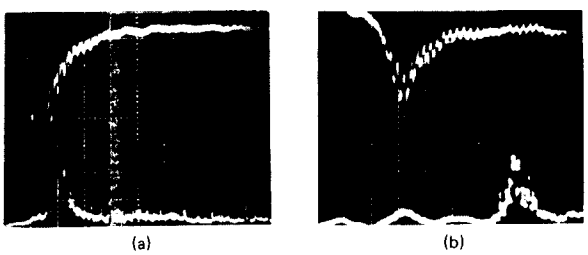

FIG. 3. Examples of (a) prompt and (b) late backscatter, the difference being caused by the level of pre-ionization. Upper traces: incident laser pulse (75 MW/div, inverted). Lower traces: backscatter (approximately 9 kW/div for prompt, 600 W/div for late). Horizontal: 50 nsec/div.

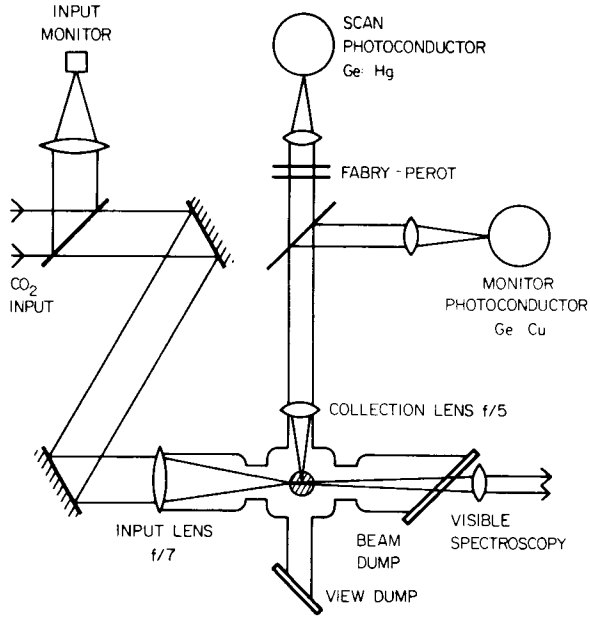

FIG. 4. Experimental arrangement used in sidescatter measurements. Backscatter is observed by adding another beam-splitter in the incident beam.

500 nsec after the CO_2 laser peak. These measured shifts are similar to the shift reported previously[13] for backscatter observed at the higher intensity of 6×10^{11} W/cm^2. There, the Brillouin nature of the backscatter was confirmed and the noise level, exponentiation rate, and saturation level were reported. The reflectivities in the present investigation are, of course, lower than those reported at the higher intensity. Power reflectivities observed for prompt and late backscatter are 1.5×10^{-4} and 2.5×10^{-5}, respectively.

B. Sidescatter observations

As with backscatter, time histories of sidescatter exhibit a dependence on pre-ionization by the arc. Shown in Fig. 5 are relative time histories of sidescatter and backscatter under conditions where prompt and late scattering are observed. Sidescatter always occurs in a short burst, 10–40 nsec long, even when observed during the tail of the laser pulse, where no

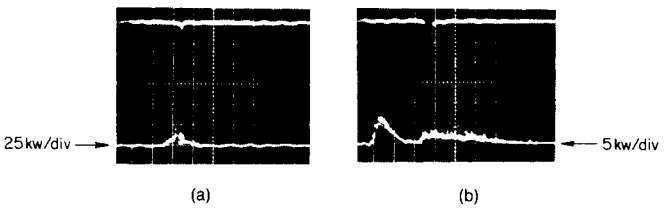

FIG. 5. Relative timing of sidescatter (upper traces, approximately 200 W/div) and backscatter (lower traces) under conditions of (a) prompt scattering (higher pre-ionization) and (b) late scattering (lower pre-ionization). Note the change in backscatter signal gain between (a) and (b), causing the stray light peak to be prominent in the lower trace of (b). Late backscatter is 25 times smaller than prompt backscatter, though the incident intensity is only 5 times smaller at late times. Horizontal: 100 nsec/div.

input variations with that time scale are observed. This property of the sidescatter leads to the hypothesis that the source of the scattering is in motion along the laser axis. Sidescatter would then be observed only while that scattering source passed through the region seen by the sidescatter detector.

To test this hypothesis, an experiment was performed (with the lesser pre-ionization) in which the two photoconductive detectors were aligned to different points along the laser axis. The time at which sidescatter occurs is found to be correlated with position; scattering occurs earlier from points nearer the input lens. The implied velocity in the direction of the incident laser wave vector is 5×10^6 cm/sec $\pm$ 50%, approximately the acoustic speed in this plasma.

The spectrum of the observed sidescatter shows a red shift of 9 ± 1.5 GHz from the incident laser frequency. This is approximately $\sqrt{2}$ less than that observed for backscatter, despite the difference between backscatter and sidescatter source regions (which will be discussed in Sec. IV). This shift is consistent with Brillouin sidescatter; but in subsequent experiments at higher intensity,[14] measurements of exponentiation, isotropy, and polarization of the sidescatter indicate that more than one mechanism is involved. Scattered light levels are very low, with power reflectivities of the order of 10^{-5} per sr.

C. Plasma diagnosis

In the absence of incident CO_2 laser radiation, the arc discharge in 15 Torr of H_2 produces a plasma with electron density $n_e=10^{16}$ cm^{-3}, as determined by Stark broadening of the H_β line. Electron temperature measured by hydrogen line-to-continuum techniques is found to be 4–5 eV. With the CO_2 laser incident as described here, neutral hydrogen line intensities become too low for diagnostic purposes, and density is determined by Stark width measurements of the He II 4686 Å line emission from 1.7 Torr of helium seed gas. Time histories of the maximum electron density on axis obtained in this manner are found to depend upon the initial level of pre-ionization. Shown in Fig. 6 are two plots of electron density versus time during the decay of the incident pulse, for two levels of pre-ionization. Note that the maximum densities measured spectroscopically with higher pre-ionization, at times soon after laser peak power, are in excess of full ionization of the fill gas by about 50%. These high values are believed to be spurious; line shapes indicate that optical depth effects may be causing overestimates of line widths. Also note that with lower pre-ionization, no spectroscopic determination of density can be made until 150 nsec after laser peak power, due to insufficient intensity of the diagnostic line.

Further information concerning temporal evolution of electron density in the laser-altered plasma, including information about the spatial distribution of the density, is obtained by ruby laser interferometry. A sequence of four interferograms taken at different times relative to the time of peak CO_2 power under

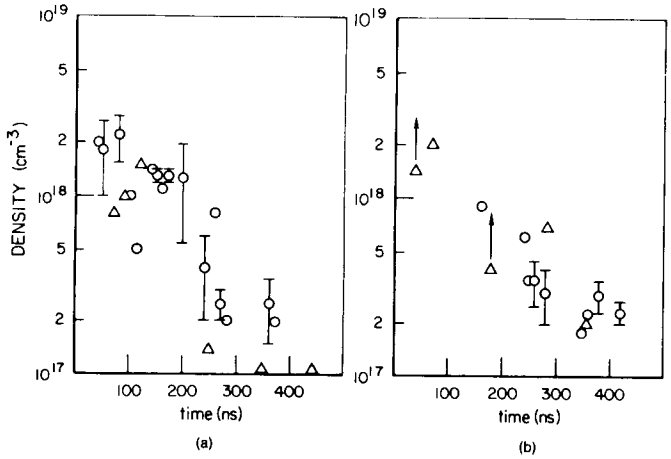

FIG. 6. Maximum electron density in the laser-altered plasma as a function of time after the peak of the incident CO_2 pulse, for (a) higher pre-ionization (prompt scatter conditions) and (b) lower preionization (late scatter conditions). Points (○) are from spectroscopy and triangles (△) are from Abel inversion of ruby interferograms.

conditions of greater pre-ionization is shown in Fig. 7. An ionization disturbance is seen to propagate into the arc plasma from the position of best CO_2 focus, which is just out of the field of view at the bottom of the interferograms. Radial expansion transverse to the CO_2 laser axis of the plasma behind the front of the ionization wave leads to the bullet-shaped nature of the disturbance. A similar set of interferograms for conditions of lower pre-ionization are shown in Fig. 8.

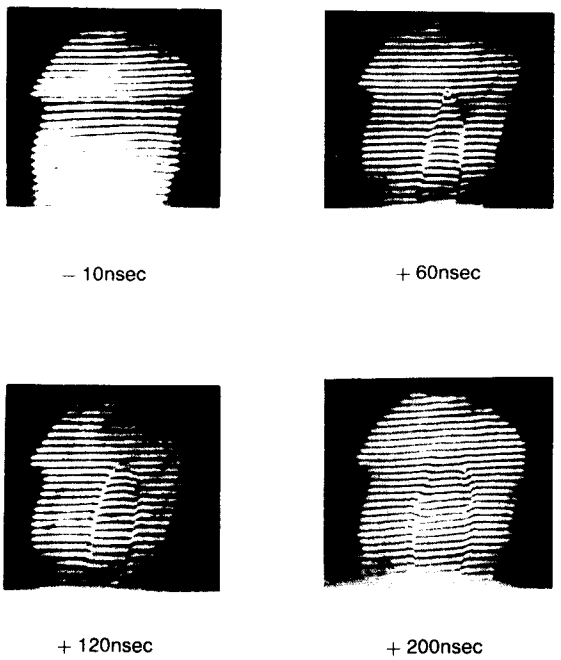

FIG. 7. Sequence of interferograms taken under higher pre-ionization conditions at four times relative to CO_2 input peak. The arc discharge axis is horizontal, and the entire field of view has an initial density $n_e = 10^{16}$ cm^{-3} due to the arc. The CO_2 beam enters at the bottom and exits at the top of the interferograms; best CO_2 focus is located just outside of the field of view at the bottom. The usual sidescatter collection axis is out of the plane of the figure. Size scale is 1.5 mm per fringe.

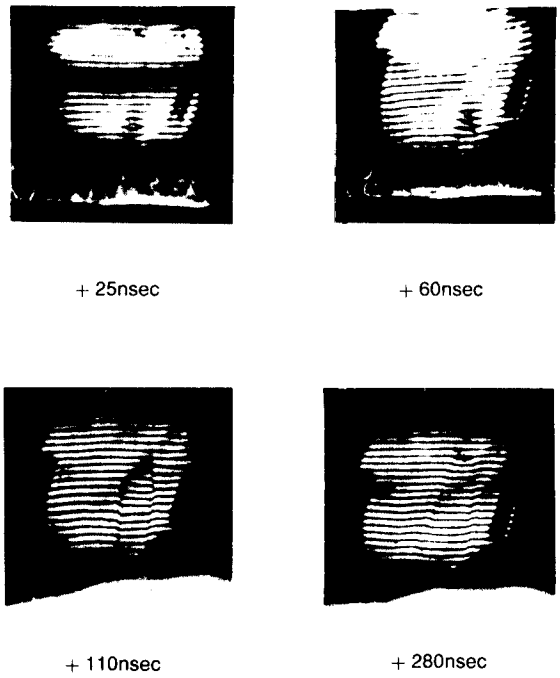

FIG. 8. Sequence of interferograms as in Fig. 7, but under conditions of lower pre-ionization.

Two major differences between Figs. 7 and 8 are evident. First, the rate at which the front of the ionization wave propagates along the laser axis is greater with more pre-ionization than with less pre-ionization. In the latter case, the axial velocity is the same, within experimental error, as the velocity inferred for motion of the late sidescatter source in Sec. IIIB. The second difference is that the ionization wave is seen to stall in the case of greater pre-ionization; axial propagation ceases just past the center of the arc at relatively early times after CO_2 input peak. With less pre-ionization, the ionization wave continues to propagate all of the way across the arc at much later times after input peak power. The importance of this observation will be evident in our discussion of the cause of late backscatter.

Quantitative densities are obtained from Abel inversion of the interferograms under the assumption of cylindrical symmetry. Shown in Figs. 9 and 10 are sequences of density plots under conditions of more and less pre-ionization, respectively. The differences mentioned here are still evident. In addition, one now sees that the radial expansion behind the front leaves a density minimum. The axial profile, then, is characterized by three distinct regions. In the front of the ionization wave is a short but dense region ($n_e \gtrsim 10^{18}$ cm^{-3}). Ahead of this front, density falls off to pre-ionization levels (10^{16} cm^{-3}), while behind the front a density of $(1.5 \pm 0.5) \times 10^{17}$ cm^{-3} is seen in an elongated region of radially expanded plasma that has been ionized and heated by the CO_2 radiation. The time history of density in the front may be compared with that obtained spectroscopically. As shown in Fig. 6, reasonable agreement is obtained between the absolute magnitudes of electron density determined by these two techniques.

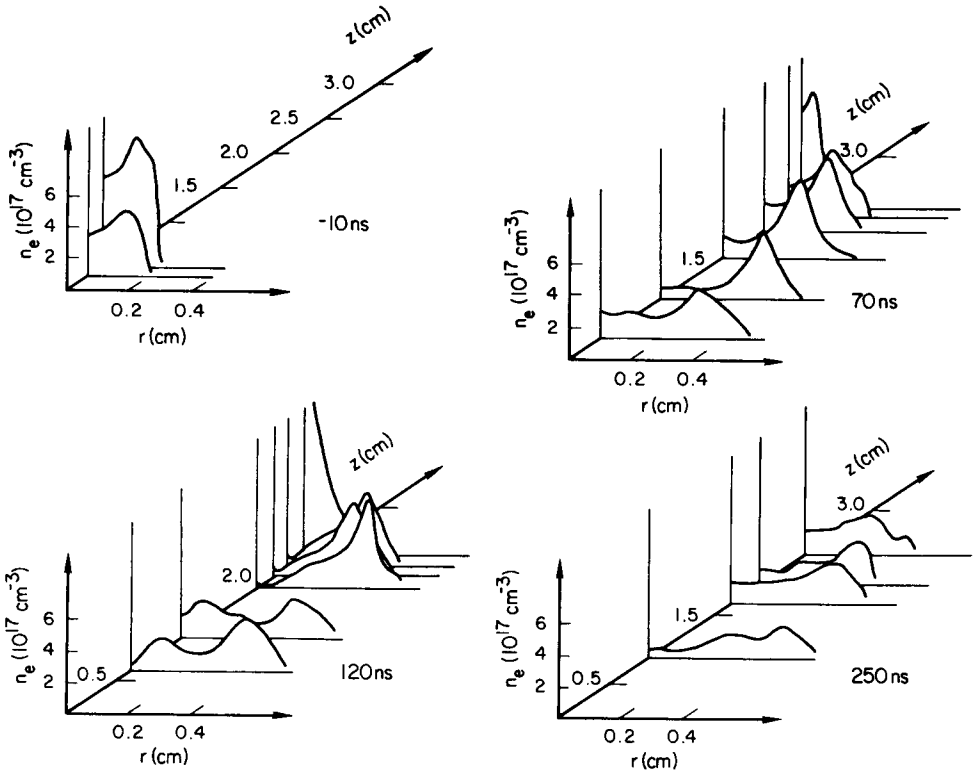

FIG. 9. Electron density profiles at four times after peak incident power, as obtained by Abel inversion of ruby interferograms. The CO_2 beam is incident in the + Z direction, and the point of best focus is at $Z = 0$. This sequence corresponds to conditions of higher pre-ionization.

D. Effect of smoothed input pulse on backscatter spikiness

Observed backscattered power, as may be seen from Fig. 3, is spiky in time, with at least some of the spikiness seemingly correlated with self-mode-locked spikes of the incident pulse. To test whether backscatter spikiness is due solely to input spikiness, observations were made of the scattering while using the smoothed CO_2 input pulses generated with cw injection into the pulsed oscillator. Smoothed input pulses and resultant backscatter appear in Fig. 2, and may be compared with the backscatter observed using spiky input pulses shown in Fig. 3. It is seen that backscatter spikiness is not solely due to input laser spikiness, since it occurs also with smoothed pulses.

IV. DISCUSSION

A. Explanation of prompt and late sidescatter

From sidescatter observations and interferometric diagnostics, it is possible to establish the source of

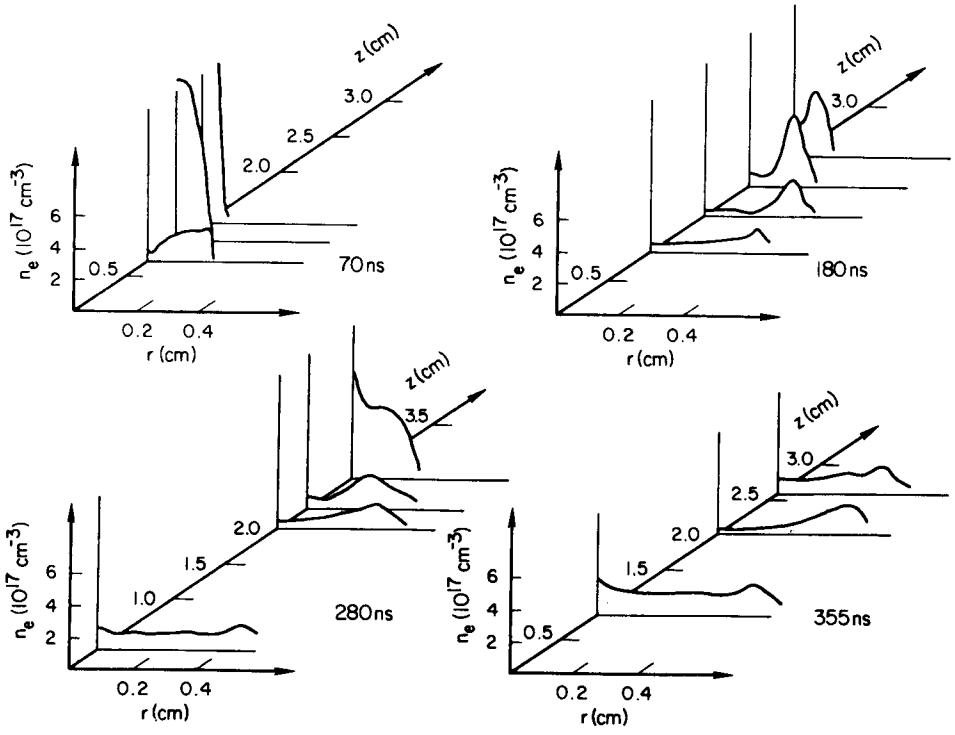

FIG. 10. Electron density profiles, similar to Fig. 9, but for conditions of lower pre-ionization.

prompt and late sidescatter. First, the sidescatter source moves, as described in Sec. IIIB, with the same velocity as the front of the ionization wave, which is seen interferometrically. In addition, the time of arrival of the front at the center of the arc, where the detection optics are focused, corresponds to the time of observed sidescatter for both prompt and late scattering. It is possible, then, to identify the dense front of the ionization wave as the source of the sidescatter. This implies that the observation of prompt and late sidescatter is coupled to the fact that the sidescatter collection volume is displaced from the best CO_2 focus, where the ionization wave starts. Later experiments performed with sidescatter collected from the best focal spot confirm that scattering is always prompt at any pre-ionization level that allows ionization to take place.

B. Explanation of prompt and late backscatter

In order to establish the cause of the prompt Brillouin backscatter, a more subtle approach is required. If the backscatter source were the same dense front of the ionization wave, one would expect there to be no dense front at early times under late backscatter conditions. From Fig. 10, however, it may be seen that such a front does exist. The difference at early times between the plasma with less pre-ionization and the plasma with more pre-ionization is that there is a much longer length of radially expanded plasma behind the front in the latter case. One may hypothesize that this is the region in which backscatter grows, in which case the greater interaction length at early times with more pre-ionization allows prompt backscatter to be seen.

To test this hypothesis, we can attempt to apply it to late backscatter. Indeed, one finds a longer region of radially expanded plasma at later times with less pre-ionization, so that backscatter does have a sufficient gain length at late times. However, one must also explain the lack of late backscatter under conditions of greater pre-ionization. Studying Figs. 9 and 10, one finds that the difference at late times between the plasma with more and less pre-ionization is that a dense front exists with less pre-ionization but not with more pre-ionization. At first this seems to imply that the dense front is the source of the backscatter, in contradiction to our finding for prompt backscatter. However, another explanation, entirely consistent with the prompt backscatter argument, exists. This is simply that with more pre-ionization a second ionization front forms at the focus and propagates back toward the incident laser. The absorption of the incident beam in that front greatly decreases the intensity of the beam at the forward propagating front, which explains the sudden cessation of forward front propagation. The intensity in the long radially expanded region behind the forward front is also severely attenuated, preventing growth of Brillouin backscatter. Experimental evidence for the strong absorption implicit in this hypothesis is found in studies of the transmitted CO_2 beam.[15] While $\frac{1}{3}$ to $\frac{2}{3}$ of the beam energy is transmitted on a given shot, time-resolved transmission measurements show instantaneous transmission of less than 5% of the incident power. Further evidence in support of this hypothesis is obtained from subsequent experiments. With the CO_2 focal spot located well within the holographic field of view, backward ionization fronts are seen to propagate. Cessation of forward front propagation often does accompany the appearance of these backward ionization fronts.

C. Backscatter spikiness

It is not possible on the basis of the present work to establish the cause of Brillouin backscatter spikiness. One can say that the simplest possible explanation, that backscatter spikes are due solely to spikes in the input pulse, is ruled out by our smooth-pulse results. In addition to the alternative explanations mentioned in Sec. I, simultaneous scatter from separate localized regions in the plasma with differing electron temperatures might account for the spikiness. Backscattered radiation from the different regions would be frequency shifted by different amounts and could beat back at the detector. The observed bandwidth of the spikiness is only 3% of the acoustic shift, so that points with temperatures differing by only 6% need to be involved in the scattering. Further work in this area will be required to determine whether any of these possible explanations is the correct one.

V. CONCLUSION

We find that the effects of ionization and heating by the incident beam control the nature of the scattering observed. The laser-altered plasma has an elongated shape with a dense but short ionization front, followed by a long, uniform region of hot plasma at lower density. The development of this plasma can be controlled by pre-ionization. Sidescatter occurs from the dense front and is of low intensity. Brillouin backscatter grows in the long, uniform region and reaches much higher intensity. When this region is formed late because of insufficient pre-ionization, late backscatter is observed. The spikiness of Brillouin scatter cannot be attributed solely to spikiness in the pump; some of the spikiness is unrelated to mode-beating and its cause cannot be found without further work.

ACKNOWLEDGMENTS

The authors wish to acknowledge useful conversations with J. J. Turechek, D. Hodges, Y. C. Lee, R. Wuerker, and A. A. Offenberger.

This work was supported by the U.S. Department of Energy, Contract EY-76-S-03-0034, P.A. 236; the Los Alamos Scientific Laboratory, Work Order X49-0027K-1; and the National Science Foundation, Grants ENG 75-16610 and ENG 77-17861.

[1] K. A. Brueckner and S. Jorna, Rev. Mod. Phys. 46, 325 (1974).
[2] J. M. Dawson, A. Hertzberg, R. E. Kidder, G. C. Vlases, H. G. Ahlstrom, and L. C. Steinhauer, in *Plasma Physics and*

Controlled Nuclear Fusion Research (International Atomic Energy Agency, Vienna, 1971), Vol. I, p. 673.
[3]K. Nishikawa, J. Phys. Soc. Jpn. **24**, 1152 (1968).
[4]J. F. Drake, P. K. Kaw, Y. C. Lee, G. Schmidt, C. S. Liu, and M. N. Rosenbluth, Phys. Fluids **17**, 778 (1974).
[5]J. J. Turecheck and F. F. Chen, Phys. Rev. Lett. **36**, 720 (1976).
[6]R. Massey, K. Berggren, and Z. A. Pietrzyk, Phys. Rev. Lett. **36**, 963 (1976).
[7]A. A. Offenberger, M. R. Cervenan, A. M. Yam, and A. W. Pasternak, J. Appl. Phys. **47**, 1452 (1976).
[8]N. H. Burnett, H. A. Baldis, G. D. Enright, M. C. Richardson, and P. B. Corkum, J. Appl. Phys. **48**, 3727 (1977).
[9]A. A. Offenberger, A. Ng, and M. R. Cervenan, Can. J. Phys. **56**, 381 (1978).
[10]W. T. Armstrong, J. Appl. Phys. **49**, 2566 (1978).
[11]R. S. Massey, Z. A. Pietrzyk, and D. W. Scudder, Phys. Fluids **21**, 396 (1978).
[12]M. R. Cervenan and A. A. Offenberger, Opt. Commun. **24**, 302 (1978).
[13]M. J. Herbst, C. E. Clayton, and F. F. Chen, Phys. Rev. Lett. **43**, 1591 (1979).
[14]M. J. Herbst, C. E. Clayton, and F. F. Chen, J. Appl. Phys. **51**, 4080 (1980).
[15]M. J. Herbst. Ph.D. thesis, University of California, Los Angeles (1979).